Applied Catalysis B: Environmental 333 (2023) 122776

Contents lists available at ScienceDirect

Applied Catalysis B: Environmental

journal homepage: www.elsevier.com/locate/apcatb

Efficient H_2O_2 production from urine treatment based on a self-biased WO_3/TiO_2-Si PVC photoanode and a WO_3/CMK-3 cathode

Lei Li [a], Jinhua Li [a,*], Fei Fang [a], Yan Zhang [a], Tingsheng Zhou [a], Changhui Zhou [a], Jing Bai [a,b], Baoxue Zhou [a,b,**]

[a] School of Environmental Science and Engineering, Key Laboratory of Thin Film and Microfabrication Technology (Ministry of Education), Shanghai Jiao Tong University, No. 800, Dongchuan Rd, Shanghai 200240, PR China
[b] Shanghai Institute of Pollution Control and Ecological Security, Shanghai 200092, PR China

ARTICLE INFO

Keywords:
Urine treatment
H_2O_2 production
Chlorine radical
Nitrogen removal

ABSTRACT

Urine accounts for only 1% of municipal wastewater volume but contributes 80% of nitrogen, which has become one of the challenges for existing wastewater treatment plants. Herein, we proposed a novel approach based on a self-biased WO_3/TiO_2-Si PVC photoanode and a WO_3-modified mesoporous carbon (CMK-3) cathode (WO_3/CMK-3) to produce significantly high-value chemical H_2O_2 from urine treatment with effective total nitrogen removal. The central idea of the design is to achieve a feasible reversal of the thermodynamic trend of O_2 reduction to H_2O_2 from a non-spontaneous to a strongly spontaneous process by combining it with a urine treatment reaction that releases large amounts of chemical energy in the photoelectrocatalytic (PEC) system. The results indicated that the H_2O_2 production was boosted remarkably by urine disposal reaction (5.13 mg cm^{-2} h^{-1}) with a faradaic efficiency of 72%, and the WO_3/CMK-3 cathode showed 6.1 and 2.5 times higher H_2O_2 production activity than the common gas diffusion electrode and carbon felt electrode, respectively. Moreover, urine was degraded effectively into N_2 with a total nitrogen removal of 91.4% within 120 min, and the kinetic constant of urine degradation was 0.0397 min^{-1}, which was 15.4 times that of the blank. The results of ESR and quenching experiments demonstrated that the amine group of urine selectively and rapidly converted into N_2 by Cl•. This study provides new insights into efficient urine disposal and synchronous H_2O_2 production.

1. Introduction

Nitrogen pollution is the main source of eutrophication in water bodies [1]. Urine, as a high-concentration nitrogenous waste, contributes 80% of the urea-N and 10% of the COD, although it accounts for only 1% of the municipal wastewater volume [2–4]. The nitrogen content in the urine wastewater is severely overloaded, which is a difficult problem for wastewater treatment [5]. Many methods have been developed for urine-N treatment, which include nitrification and denitrification [6], reverse osmosis [7], and adsorption [8]. However, these methods still suffer from secondary contamination, low efficiency, high energy consumption and operational complexity [9–12]. The advanced oxidation processes driven by the photoelectrochemical method have also been used for urea treatment because of their effectiveness, operational simplicity, and environmental friendliness [13,14]. Moreover, it is driven by electricity from renewable sources, such as solar and wind, providing a green and sustainable alternative to conventional treatment processes [15]. However, urea is rich in chemical energy and its simple oxidation is an exothermic process, which will result in a large amount of released chemical energy that cannot be recovered. Therefore, how to design systems for recovering chemical energy directly from urine treatment is extremely attractive [16,17].

Recently, hydrogen generation by electrolysis of urine wastewater has attracted wide attention. Since the oxidation of urea to produce H_2 requires a lower potential (0.37 V) compared to water splitting, this process can significantly reduce the thermodynamic difficulties of hydrogen production, which can significantly reduce energy consumption [18,19]. Moreover, urea is an abundant source of hydrogen (~6.71 wt%), which means that the hydrogen energy in it can be efficiently recovered [20,21]. However, the process of Eq. (1) remains a

* Corresponding author.
** Corresponding author at: School of Environmental Science and Engineering, Key Laboratory of Thin Film and Microfabrication Technology (Ministry of Education), Shanghai Jiao Tong University, No. 800, Dongchuan Rd, Shanghai 200240, PR China.
E-mail addresses: lijinhua@sjtu.edu.cn (J. Li), zhoubaoxue@sjtu.edu.cn (B. Zhou).

https://doi.org/10.1016/j.apcatb.2023.122776
Received 15 November 2022; Received in revised form 30 March 2023; Accepted 17 April 2023
Available online 18 April 2023

thermodynamically non-spontaneous tendency, which requires additional energy, thus limiting the development of urine wastewater electrolysis. In terms of thermodynamics (Eq. (2)), the decomposition of urea in O_2 can release a large amount of chemical energy (1343.2 $kJ{\cdot}mol^{-1}$), which means that urine is a rich reservoir of energy.

$$CO(NH_2)_2\ (urea) + H_2O \rightarrow N_2 + CO_2 + 3\ H_2,\ \Delta G_0 = 40 kJmol^{-1} \quad (1)$$

$$2\ CO(NH_2)_2 + 3\ O_2 \rightarrow 2\ CO_2 + 2\ N_2 + 4\ H_2O,\ \Delta G^0 = -1343{\cdot}2\ kJ{\cdot}mol^{-1} \quad (2)$$

In additon, urea oxidation reaction (UOR) involves complicated $6e^-$ transfer and is prone to excessive oxidation to nitrate and nitrite, leading to incomplete denitrification and secondary contamination [22]. Fortunately, recent studies have proposed to use the characteristics of high selectivity and strong oxidation of chlorine radicals (Cl•, ClO•) [23–25] to oxidize the electron-rich amine (ammonia)-nitrogen groups, which aimed to achieve simultaneous chemical energy recovery from the urine treatment process in the photoelectrochemical system and obtained satisfactory results [26,27]. On this basis, a novel electrochemical system mediated by Cl• is constructed, where Cl• is used as an electron mediator for the oxidative denitrogenation of urea.

Hydrogen peroxide (H_2O_2), as a well-known green and environmentally friendly water treatment agent [28,29], which is widely used in the chemical, food, and pharmaceutical industries. In recent years, a series of H_2O_2 preparation methods have been developed, among which the most studied is the oxygen reduction method. However, the H_2O_2 production by oxygen reduction is a thermodynamically non-spontaneous process, which is highly energy intensive [30]. For this reason, we imagine that if the urine oxidative denitration process can combine with the H_2O_2 preparation process, i.e., Eq. (2) + Eq. (3), a new chemical reaction can be formed (Eq. (4)), which is a process with a strong thermodynamic spontaneous trend. This means that the chemical energy released from urine disposal can be effectively recovered by the reduction of O_2 to produce H_2O_2.

$$2\ H_2O + O_2 \rightarrow 2\ H_2O_2,\ \Delta G^0 = +\ 238{\cdot}162 kJmol^{-1} \quad (3)$$

$$2\ CO(NH_2)_2 + 5\ O_2 \rightarrow 2\ CO_2 + 2\ N_2 + 4\ H_2O_2,\ \Delta G^0 = -866{\cdot}876 kJmol^{-1} \quad (4)$$

Based on the above consideration, we presented a novel method based on a self-biased WO_3/TiO_2-Si PVC photoanode and a WO_3/CMK-3 cathode to significantly produce the high value-added chemical H_2O_2 from urine treatment with efficient total nitrogen removal. A WO_3-modified mesoporous carbon electrode (WO_3/CMK-3) served as the cathode on account of its high specific surface area and hydrophilic/hydrophobic interface, which can give it a large number of catalytic active sites and efficient O_2 transfer channels for efficient H_2O_2 production. A self-biased composite photoanode was employed as the anode (WO_3/TiO_2-Si PVC) to strengthen the generation of Cl• for highly selective removal of total nitrogen from urine, which was constituted by front WO_3/TiO_2 photoanode and rear polycrystalline silicon cell (Si PVC). Electrons generated from the oxidation of urine were then transported to the cathode for H_2O_2 production. We first investigated the H_2O_2 production performance of the WO_3/CMK-3 cathode and then evaluated the H_2O_2 production from synthetic urine treatment. Meanwhile, the total nitrogen removal efficiencies of synthetic urine and actual urine were also been assessed. ESR analysis and quenching experiments were performed to investigate the mechanism of Cl• production for urine degradation. This work offers new perspectives on effective urine treatment and synchronous H_2O_2 generation.

2. Experimental

2.1. Chemicals and materials

Mesoporous carbon CMK-3 was purchased from XFNANO (Nanjing, China). Nafion 117 membrane and Nafion dispersions were purchased from Dupont. Carbon paper material (CP) was obtained from Keqi (Shanghai, China). Other chemical reagents of analytical grade used in the study were obtained from Macklin. Deionized water (DI, ≥18.25 MΩ·cm) was utilized for the preparation/dilution of all samples.

2.2. Fabrication of the WO_3/CMK-3 cathode

Firstly, the WO_3 nanoparticle supported on mesoporous carbon CMK-3 was prepared by the polymeric precursor method (PPM) [31], in which tungsten chloride was used to find the best tungsten proportion. Then, the WO_3-loaded CMK-3 catalyst was spray-coated on the commercial CP to obtain a catalytic layer (0.653 mg cm^{-2}). The schematic diagram of the fabrication process of the WO_3/CMK-3 cathode was shown in Fig. S1. The CP was immersed in PTFE suspension (2%, v/v) for 10 min, dried in the oven, and then calcined at 360 °C for 0.5 h to form a super-hydrophobic gas diffusion layer. A catalyst suspension containing 20 mg CMK-3, 125 μl Nafion solution (5 wt%), 5 mL ethanol, and 1 mL DI water was sequentially homogenized by stirring and ultrasonic treatment for 1 h. Then, 2 mL of the homogenized suspension was spray-coated on the CP and dried at room temperature. After calcining at 360 °C for 0.5 h, the WO_3/CMK-3 cathode was obtained (1 × 1 cm^2).

2.3. Construction of the WO_3/TiO_2-Si PVC photoanode

The WO_3/TiO_2 nanoplate photoanode was fabricated by a hydrothermal synthesis method [32,33], and the detailed procedure was shown in Fig. S2. A commercial silicon photovoltaic cell pack (Si PVC, 3.7 × 6.8 cm^2) connected in series by copper strip and Ag epoxy was used as the rear photoanode. The positive pole of Si PVC was connected to the back of the WO_3/TiO_2 photoanode by copper wire and then sealed via silicone rubber to form a composite photoanode. The illustration of the WO_3/TiO_2-Si PVC photoanode in the PEC system was displayed in Fig. S3.

2.4. Experimental setup

As shown in Fig. 1, the photoelectrocatalytic experiments for synthetic urine treatment and simultaneous H_2O_2 generation were performed in a flow cell reactor with a two-electrode system, where WO_3/CMK-3 and WO_3/TiO_2-Si PVC were used as the cathode and photoanode, respectively. A 300-W Xe lamp with an AM 1.5 filter (PerfectLight, China) was applied for light illumination (100 mW cm^{-2}). The reactor contains three chambers, in which the anodic chamber was fed with a solution containing 30 mg L^{-1} urea, 0.1 M Na_2SO_4 and 0.05 M NaCl, the cathodic chamber was supplied with 0.1 M Na_2SO_4, and the gas chamber was flushed with continuous O_2 flow. The anodic and cathodic chambers were separated by a proton exchange membrane (PEM, Nafion 117). The anolyte was circulated to evaluate the accumulated urea degradation, and the catholyte flowed in a single pass to bring out the synthesized H_2O_2 at a flexible rate. All experiments were carried out in an electrochemical workstation (CHI 660c, China). Samples were taken at regular intervals to determine urea, nitrate nitrogen, ammonia nitrogen and total nitrogen in the anodic chamber and hydrogen peroxide in the cathodic chamber. The quantification of H_2O_2 was carried out by the potassium titanium oxalate method [34], which was measured by a UV−vis spectrophotometer (752 N, INESA, Shanghai) at 410 nm. The actual urine wastewater was collected from the public latrines. After filtering (0.45 μm) and diluting to the appropriate concentration (physicochemical properties were shown in Table S2), it was treated with the same device.

2.5. Analytical methods

The surface morphology and composition of electrodes were determined by high-resolution transmission electron microscopy (HRTEM, JEOL-2100 F/F200) and a scanning electron microscopy (SEM, Zeiss SUPRA55-VP) equipped with an X-ray energy dispersive spectrometer

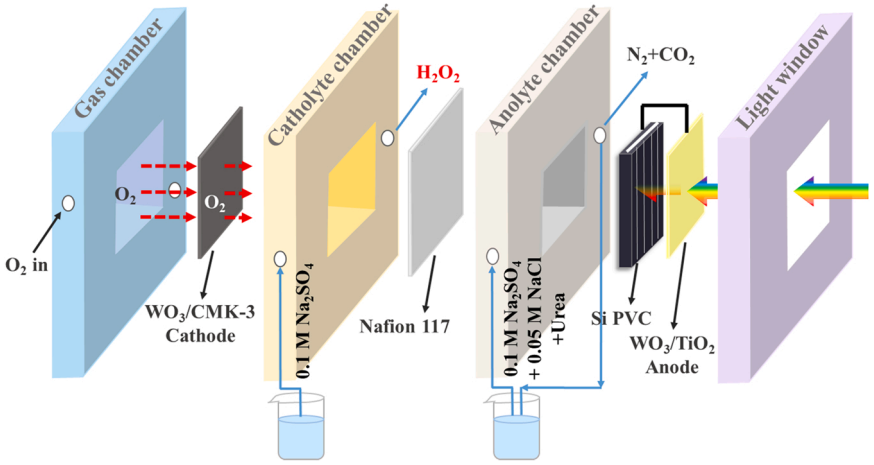

Fig. 1. Schematic illustration of the PEC system for efficient H_2O_2 production from urine treatment.

(EDS). X-ray diffraction (XRD, Rigaku D-Max B) was used to measure the crystal structure of the electrodes. The elemental compositions of electrodes were analyzed with an X-ray photoelectron spectroscopy (XPS, AXIS Ultra DLD). Brunaure–Emmett–Teller (BET) surface area and pore-size distributions were measured using N_2 adsorption–desorption isotherms (Autosorb-iQ/ASAP 2460). The Fourier transform infrared (FT-IR) spectra were collected on a Thermo Nicolet 6700 spectrometer (U. S.). The contact angle of the sample was characterized with a drop shape analyzer (KRUSS, Germany, DSA100). Linear sweep voltammetry (LSV) and cyclic voltammetry (CV) were performed in a three-electrode system at a scan rate of 50 mV s^{-1} in 0.1 M Na_2SO_4 solution. The free radical species were determined using the electron spin resonance method (ESR, LP920).

The rotation ring disk electrode (RRDE) tests were performed in a typical three-electrode cell with a reference electrode of Ag/AgCl. A RRDE assembly (AFMSRCE, Pine Instruments) consisting of a glassy carbon rotating disk electrode (area = 0.2472 cm^2) and a Pt ring (area = 0.1859 cm^2) was used as a working electrode with a theoretical collection efficiency of N = 0.389. To prepare the working electrode, a solution containing 10 mg of catalyst was mixed with 3 mL of isopropanol and 30 μL of Nafion 117 solution and sonicated for 20 min to obtain a homogeneous catalyst ink, and then 6 μL of the ink was painted onto the glassy carbon disk to obtain a catalyst loading of 0.08 mg cm^{-2}. The H_2O_2 molar selectivity can be calculated by the following equation:

$$H_2O_2 \quad molar \quad selectivity = \frac{i_r/N}{i_r/N + i_d} \times 200$$

where i_r and i_d represent the ring current and disk current (mA), respectively.

Urea concentration was determined by high-performance liquid chromatography (HPLC-2010 Plus, Shimadzu). The concentration of ammonia nitrogen was determined by Nessler's reagent colorimetric method, and the absorbance at 420 nm was measured using a UV–vis spectrophotometer (TU-1901, Pgeneral). Nitrate and nitrite were determined using ion chromatography (ICS-5000 +/900). TN was determined using a TN/TOC analyzer (Analytik Jena). The generated N_2 was analyzed by a gas chromatograph (GC9790 Plus, China).

3. Results and discussion

3.1. Characterization of the electrodes

To realize efficient mass transfer and catalytic reduction of O_2, a novel gas diffusion cathode with the hydrophilic/hydrophobic interface was designed (WO_3/CMK-3). The WO_3/CMK-3 cathode was composed of a gas diffusion layer and a catalytic layer, and the preparation process was illustrated in Fig. S1. Carbon paper was used as the gas diffusion layer because of its abundant macropore and microporous structure (Fig. S4), which endows it with fast gas permeation and low gas diffusion resistance. To prevent carbon paper from water flooding and further improve its oxygen diffusion performance, the superhydrophobic modification of carbon paper using PTFE was performed. And the water contact angle measurement results showed that the PTFE-modified CP exhibited prominent hydrophobicity with a water CA of 143° (Fig. S5 (a)). Mesoporous carbon CMK-3 was used as the catalyst substrate due to its large BET surface area, abundant defect active sites, and positive zeta potential, which endows it with excellent selectivity for H_2O_2 production [35,36]. To further strengthen the catalytic activity of CMK-3 for H_2O_2 production, the WO_3 modification on CMK-3 proceeded owing to its loading on CMK-3 may improve the activity and selectivity by introducing a large number of oxygen-containing functional groups and increasing the hydrophilicity of the catalyst surface [31,37]. The CA results (Fig. S5(b)) confirmed the excellent hydrophilicity of the catalytic layer (88.8°). The surface morphology of the WO_3-modified CMK-3 cathode is displayed in Fig. 2(a), which exhibits a loose skeleton and a hierarchical porous structure. The EDS mappings of the WO_3/CMK-3 cathode are shown in Fig. 2(b), which illustrates the existence and uniform dispersion of C, O and W on the selected architecture. The TEM images show that WO_3 is uniformly dispersed on CMK-3 (Fig. 2(c)), and a lattice fringe of 0.388 nm is clearly observed (Fig. 2(d)), corresponding to the (002) crystal plane of WO_3. With the increase of the WO_3 modification ratio, the more obvious WO_3 agglomeration (Fig. S6(a)–(d)). The XRD patterns of the WO_3/CMK-3 cathodes with different W proportions (w/w) are displayed in Fig. 2(e), clearly showing the characteristic peaks at 2θ = 23.1, 23.6, and 24.4°, corresponding to the (002), (020) and (200) crystalline planes of WO_3, respectively. This indicated that the WO_3 was successfully modified on CMK-3 according to JCPDF #20–1323. To further investigate the structure and porosity of different WO_3-modified catalysts, the adsorption-desorption isotherms of N_2 were analyzed. As depicted in Fig. 2(f), the isotherms were all type IV, which confirmed the coexistence of micropores, mesopores, and macropores. As the amount of WO_3 increased, the BET surface areas decreased from 1297.71 to 689.98 m^2 g^{-1}, and the pore volume decreased from 2.66 to 1.46 cm^3 g^{-1} (Table S1), which may be ascribed to the formation of WO_3 nanoparticles on CMK-3 pores. Micropores provide active sites for oxygen reduction reaction (ORR), but mesopores and macropores serve as gas transfer channels to supply oxygen [38]. Besides, it can be observed that the WO_3 modification did not change the morphology and size of CMK-3 (Fig. S7). These results indicated that the large BET surface area and abundant pore structure give the WO_3-modified CMK-3 a large number of exposed catalytic sites, which is conducive to the reduction of O_2 to produce H_2O_2 [39].

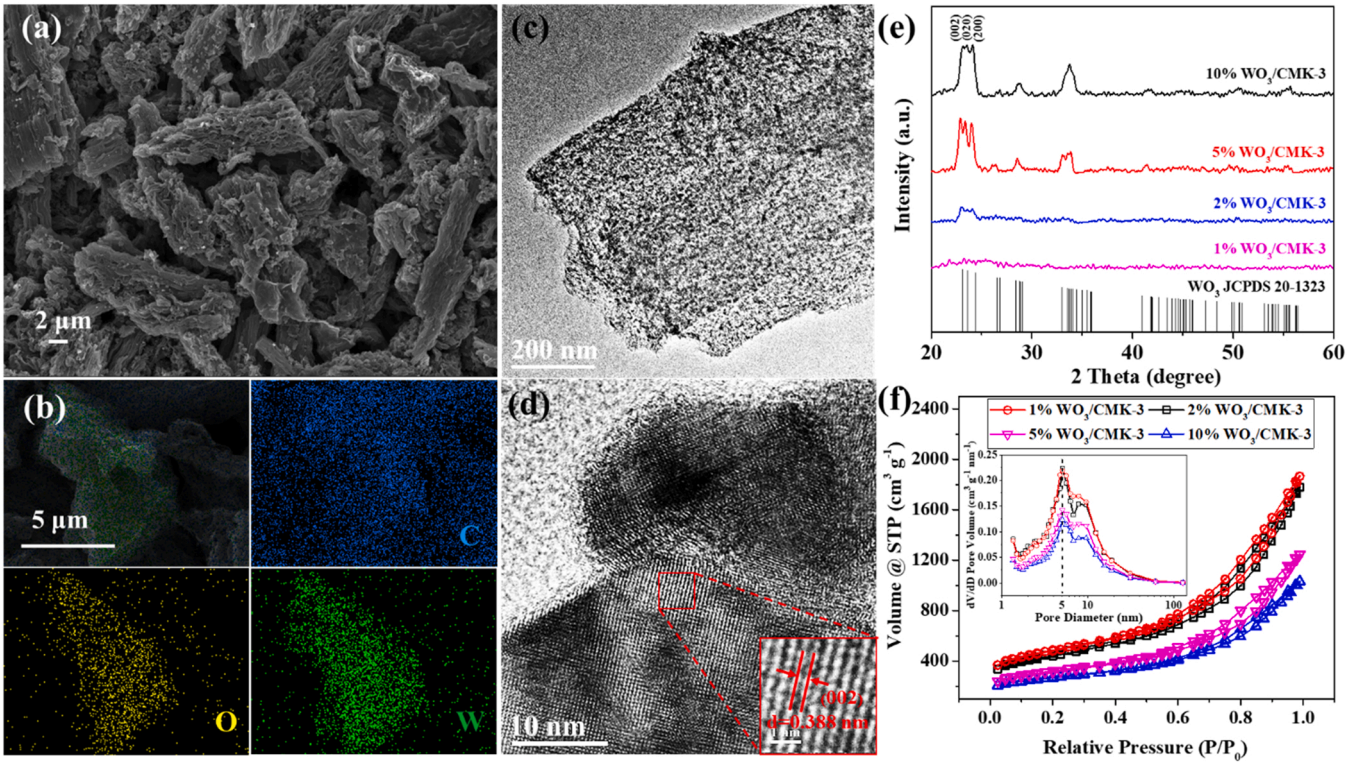

Fig. 2. SEM image of (a) WO_3/CMK-3 cathode. (b) EDS elemental mappings of C, O, and W. (c)-(d) TEM images of WO_3/CMK-3 at different magnifications. (e) XRD patterns of WO_3/CMK-3 catalysts with different W proportions (w/w). (f) N_2 adsorption–desorption isotherms and pore-size distribution (inset) of catalytic layer materials with different W proportions (w/w).

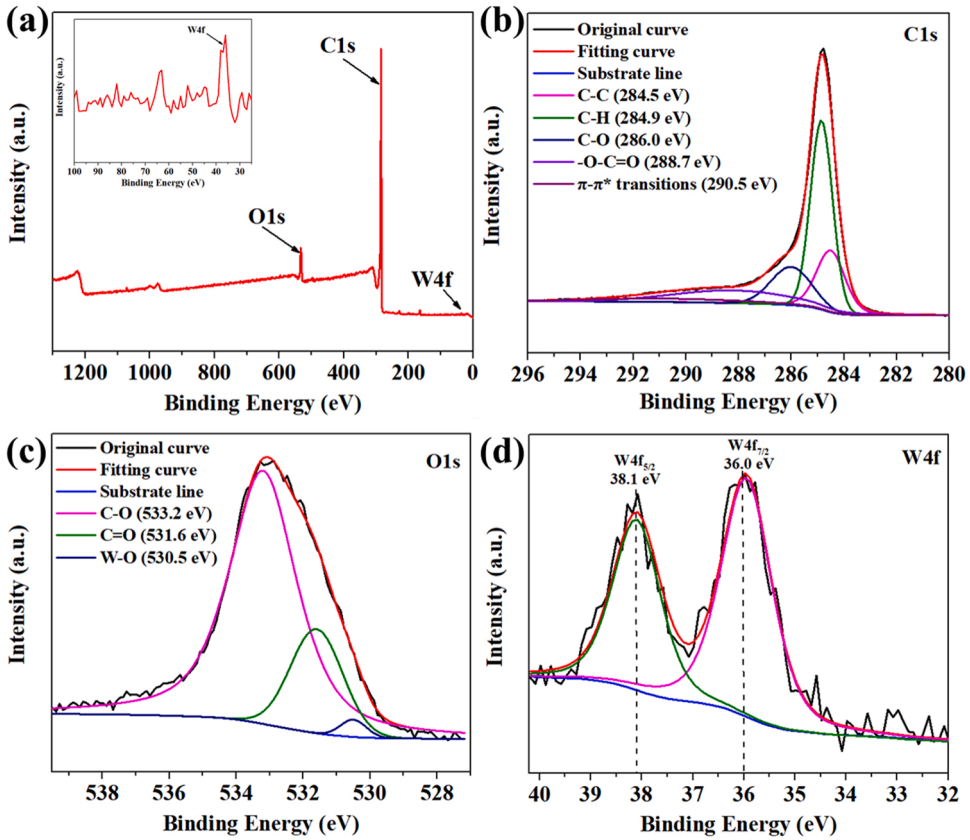

Fig. 3. (a) XPS spectra of WO_3/CMK-3 cathode. Deconvoluted (b) C 1 s, (c) O 1 s, and (d) W 4 f spectra of WO_3/CMK-3 cathode.

XPS was used to investigate the surface elemental compositions and chemical bonding states of the WO_3/CMK-3 cathode. The survey spectra demonstrated the strong peaks assigned to C 1 s, O 1 s, and W 4 f, further indicating the successful modification of W on the CMK-3 catalyst (Fig. 3 (a)). The C 1 s spectra of the WO_3/CMK-3 (Fig. 3(b)) can be deconvoluted into the following bands: graphite carbon (C-C) at 284.5 eV, C–H bond at 284.9 eV, C–O bond at 286.0 eV, carboxyl O–C═O at 288.7 eV and the characteristic shakeup line of carbon at 290.5 eV (π–π * transition) [37]. The deconvolution of the O 1 s spectra (Fig. 3(c)) showed four independent peaks: oxygen singly bound to carbon (C–O) at 533.2 eV, oxygen doubly bound to carbon (C═O) at 531.6 eV and W-O bond (derived from WO_3 modified on CMK-3) at 530.5 eV. In the W 4 f region (Fig. 3(d)), the spectra had two independent peaks at 36.0 eV and 38.1 eV, and the interval is 2.1 eV, which is consistent with the standard spectra of WO_3. In addition, Fig. S8 depicts the XPS survey scans of CMK-3 modified with and without WO_3, which exhibited a significant enhancement in the oxygen content of WO_3-modified CMK-3. These results confirmed that the WO_3 modification induced more oxygenated functional groups (such as C–OH, -C═O, and C–OOH, etc.), which could be further demonstrated by the FT-IR results in Fig. S9).

The morphology of the synthesized WO_3/TiO_2 photoanode was displayed in Fig. 4. As shown in the SEM results, WO_3 and WO_3/TiO_2 exhibited staggered plate-like structure (Fig. 4(a)-(d)), and TiO_2 was epitaxially grown on the surface of WO_3 in the form of nanoprickle. Besides, the EDS mappings shown in Fig. 4(e) demonstrated the existence and uniform dispersion of W, O and Ti on the selected architecture. High-resolution transmission electron microscopy (HRTEM) image of WO_3/TiO_2 show that the thickness of the TiO_2 nanoprickle overlayer is ~ 50 nm (Fig. 4(f)), and a typical lattice fringe spacing of 0.238 nm is observed (Fig. 4(g)), corresponding to the (004) crystal plane of anatase TiO_2 [32,40]. The XPS spectra results of WO_3/TiO_2 showed two characteristic peaks of anatase at 459.2 and 465.0 eV (as shown in Fig. S10), which further confirmed the successful modification of TiO_2 on WO_3. In addition, the XRD results suggested that WO_3 primarily grew on the FTO substrate in the form of a triclinic crystalline phase, and TiO_2 grew on WO_3 in the form of anatase with a characteristic peak of 25.3° (Fig. 4

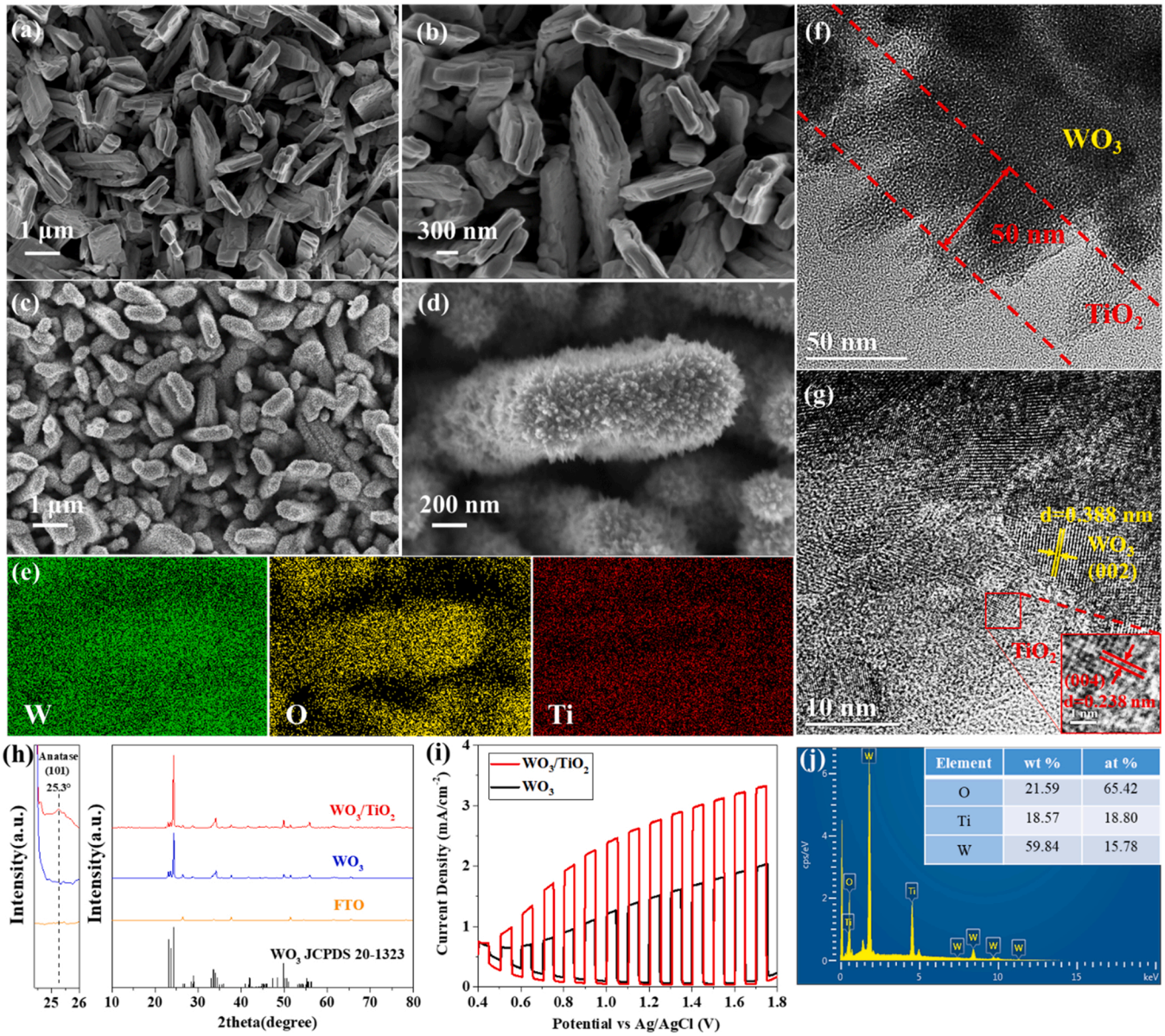

Fig. 4. SEM images of (a)-(b) WO_3 and (c)-(d) WO_3/TiO_2 electrodes at different magnifications. (e) EDS elemental mappings of W, O and Ti. (f)-(g) HRTEM image of WO_3/TiO_2 electrodes. (h) XRD patterns and (i) chopped J-V curves (scan rate 5 mV s^{-1}) of WO_3 and WO_3/TiO_2 electrodes. (j) EDS atomic ratio of W, O and Ti WO_3/TiO_2 electrode.

(h)). To assess the PEC performance of the photoanodes, the chopped photocurrent-potential (J-V) plots of WO_3 and WO_3/TiO_2 photoanodes have been investigated under AM 1.5 light (100 mW cm^{-2}) irradiation (Fig. 4(i)). The results showed that WO_3/TiO_2 electrode possesses an excellent photocurrent density of ~1.86 mA cm^{-2} at 1.23 V vs. RHE (reversible hydrogen electrode), which is 2.07 times of the WO_3 electrode (~0.9 mA cm^{-2}). This indicated that the WO_3/ TiO_2 photoanode has better charge separation and collection performance, which can be ascribed to multiple factors. Firstly, the type-II heterojunction interfacial band structure of WO_3/TiO_2 photoanode reduces the possibility of surface trap recombination and improves the separation of electron-hole pairs. Meanwhile, the feature that TiO_2 can absorb UV light also ensures its enhanced charge transport properties for WO_3 by generating charge carriers [41,42]. Moreover, the large surface curvatures of the TiO_2 nanoprickle can significantly strengthen its local electric field, and then selectively transfer the hole to the nanoprickle end. The coverage of TiO_2 can also hinder the formation of peroxotungstate on the WO_3 surface and prevent the passivation of WO_3, and then enhance the charge transfer at its interface with the electrolyte [32]. In addition, stability tests of the photoanodes were performed at different pH conditions. The results showed that TiO_2/WO_3 was superior to WO_3 alone (Fig. S11), which may be due to the modification of TiO_2 can completely seal the surface of WO_3, thus greatly improving the corrosion resistance of the anodes [43]. All these results indicated the superiority of WO_3/TiO_2 over WO_3 photoanode, which can adapt to stricter reaction conditions.

3.2. Hydrogen peroxide production

As mentioned above, we have constructed a novel photoelectrocatalytic system with self-biased WO_3/TiO_2-Si PVC as photoanode and WO_3/CMK-3 as cathode, which is used to produce H_2O_2 from synergistic urine treatment. To investigate the efficiency of H_2O_2 synthesis on the WO_3/CMK-3 cathode in this system, the yield of H_2O_2 and faradaic efficiency (FE) were assessed. As shown in Fig. S12(a), the WO_3/CMK-3 cathode showed a significantly high H_2O_2 yield of 1.16 mg cm^{-2} h^{-1} under the normal aeration (O_2 diffused through the electrolyte), which is much higher than that of the CP (0.38 mg cm^{-2} h^{-1}) and CMK-3 cathode (0.53 mg cm^{-2} h^{-1}). In addition, the FE of the WO_3/CMK-3 cathode reached 33.8%, which was 17.6% and 11.8%

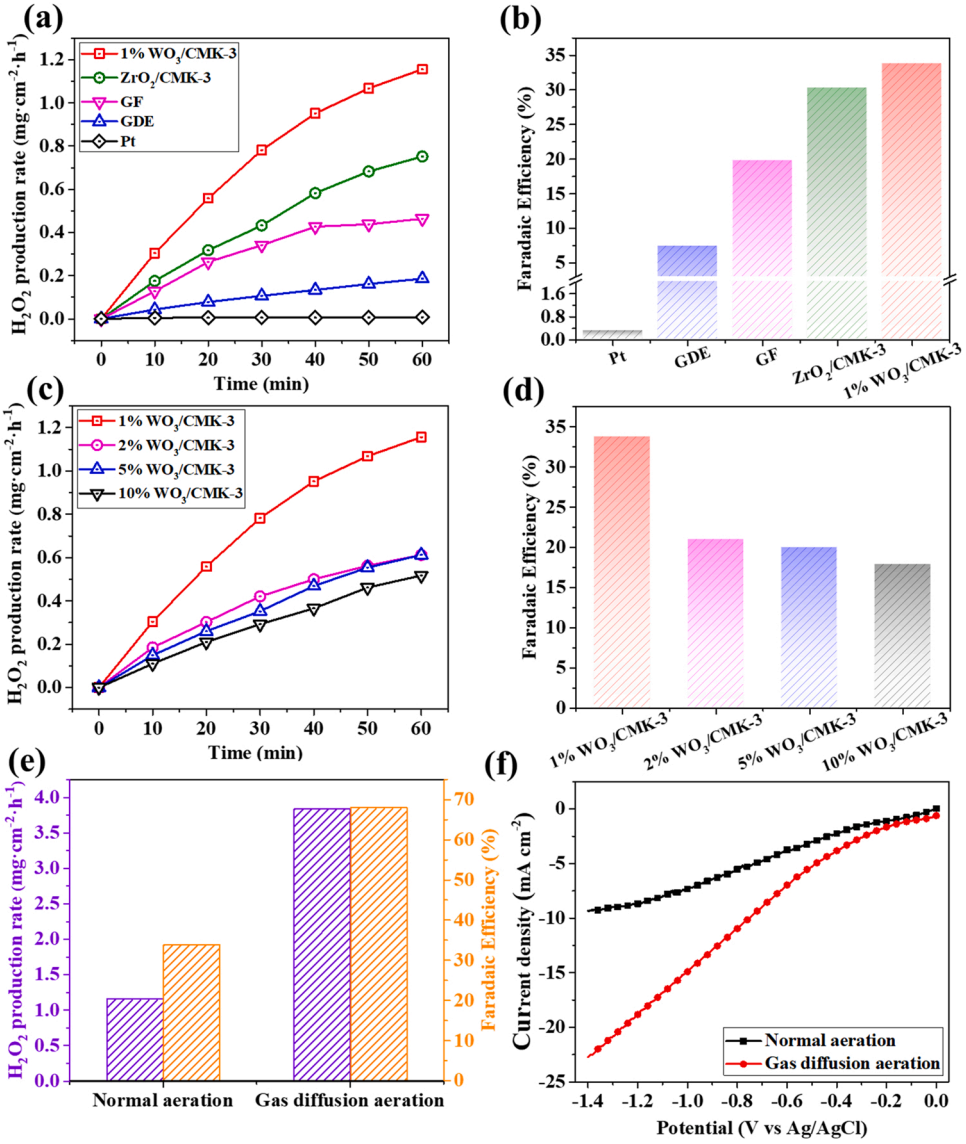

Fig. 5. (a) H_2O_2 yield and (b) Faradaic efficiency of different cathodes; (c) H_2O_2 yield and (d) Faradaic efficiency of WO_3/CMK-3 cathodes with different W proportions (w/w); Conditions : pH= 2, 0.1 M Na_2SO_4, normal aeration. Effects of (e) aeration modes on H_2O_2 yield, Faradaic efficiency, and (f) current density of 1% WO_3/CMK-3 cathode. Conditions: pH= 2, 0.1 M Na_2SO_4, gas diffusion aeration.

higher than that of the CP (16.2%) and CMK-3 cathode (22.0%), respectively (Fig. S12(b)). We then monitored the current and found the largest value for the WO_3/CMK-3 cathode (Fig. S12(c)), corresponding to its best H_2O_2 production performance. A comparison of the performance of similar PEC systems for photocatalytic production of H_2O_2 has been summarized in Table S3. Compared with the PEC systems in other studies, the WO_3/CMK-3 cathode of our system proposed in this study exhibited significant superiority in H_2O_2 generation. In addition, the current response of the prepared cathodes was significantly enhanced, indicating that the catalytic activity of H_2O_2 production was improved by incorporating the WO_3 into the CMK-3 surface. As analyzed by XPS and FT-IR results, WO_3 modification can form a large number of oxygen-containing functional groups on the CMK-3 surface, thus increasing the catalytic activity for H_2O_2 production [37]. Moreover, due to the presence of Lewis and Brunsted acid sites associated with W^{6+} species, the modification of WO_3 can make the catalyst surface exhibit acidity, and then exhibit a higher affinity for species with OH^-, which in turn provide more hydrophilicity and then accelerate the formation of the gas-liquid-solid three-phase interface [44]. The hydrophilic modifications can not only promote the transfer of reactants (H^+) and products (H_2O_2) on the catalyst interface [45], but also favor the adsorption of O_2 according to the Pauling model, which can greatly improve the selectivity of H_2O_2 generation [44].

The H_2O_2 generation activity on WO_3/CMK-3 cathode was also compared with ZrO_2/CMK-3, graphite felt (GF), common gas diffusion electrode (GDE) and Pt. As depicted in Fig. 5(a), the WO_3/CMK-3 cathode exhibited the best H_2O_2 generation performance (1.16 mg cm^{-2} h^{-1}), which was 1.6, 2.5 and 6.1 times than that of the ZrO_2/CMK-3 (0.75 mg cm^{-2} h^{-1}), GF (0.46 mg cm^{-2} h^{-1}) and GDE (0.19 mg cm^{-2} h^{-1}), respectively. However, the H_2O_2 yield on Pt was negligible (0.01 mg cm^{-2} h^{-1}). In addition, Fig. 5(b) showed that the WO_3/CMK-3 cathode presented the highest Faradaic efficiency of 33.8%, while the ZrO_2/CMK-3, GF, GDE, and Pt cathode corresponded to 30.3%, 19.8%, 7.4%, and 0.3%, respectively. All these results demonstrated that the WO_3/CMK-3 cathode possesses the outstanding performance of H_2O_2 generation, which could be attributed not only to the ordered mesoporous structure of CMK-3 ensuring abundant catalytic active sites and potential scalability toward H_2O_2 generation but also to the hydrophilic modification of CMK-3 using WO_3 ensuring excellent two-electron ORR selectivity.

To explore the optimal W ratio in WO_3/CMK-3 cathodes for H_2O_2 production, a series of experiments were conducted. As shown in Fig. 5 (c), the highest H_2O_2 production rate (1.16 mg cm^{-2} h^{-1}) was achieved for 1% WO_3/CMK-3 cathode. As the proportion of W increased, the H_2O_2 production rate significantly decreased. In the comparison of Faradaic efficiency (Fig. 5(d)), the 1% WO_3/CMK-3 cathode was also the highest (33.8%), and this trend was consistent with the H_2O_2 production. These results can be attributed to the decrease in specific surface area and pore volume of the catalytic layer due to the increased amount of WO_3 (Fig. 2 (f) and Table S1), resulting in a decline in the active sites and O_2 transport channels. Moreover, as mentioned in the work of S.N. Eroi, the excessive addition of WO_3 may lead to the degradation of peroxides, which may be another reason for the lower H_2O_2 yield of CMK-3 at higher WO_3 loading [46]. In addition, it has also demonstrated that lower content of metal loading on carbon catalysts is more active for hydrogen peroxide generation [47]. To further compare the intrinsic $2e^-$-ORR performance of carbon catalysts with different W proportions (w/w), RRDE tests were carried out in 0.1 M Na_2SO_4 solution. The catalyst was homogeneously coated on a glassy carbon disc electrode with a mass loading of 0.08 mg cm^{-2}. The electrolyte solution was pre-saturated with O_2 before each test. To allow efficient H_2O_2 diffusion into the Pt ring and to minimize H_2O_2 decomposition, the rotational speed was fixed at 1600 rpm. As shown in Fig. S13(a), among all of the catalysts studied, the 1% WO_3/CMK-3 exhibited the highest ring current, which corresponds to the best activity and selectivity for H_2O_2 production (Fig. S13(b)). Such trend in RRDE indicate a higher H_2O_2 yield for 1% WO_3/CMK-3, which is consistent with the previous TEM and BET analysis results.

As the electrode can only capture dissolved oxygen in an aqueous solution under normal aeration, and the O_2 solubility in an aqueous solution is very low (about 8 mg L^{-1} at ambient temperature and pressure), the reduction reaction of O_2 on the electrode surface will be greatly limited by oxygen transfer. Once the optimal cathode catalyst for H_2O_2 generation was determined, the investigation of the effect of gas diffusion modes on H_2O_2 production was highly necessary. Fig. 5(e) compared the H_2O_2 yield and Faradaic efficiency of the 1% WO_3/CMK-3 cathode for the photoelectrocatalytic system in different aeration modes. As the results showed, the H_2O_2 yield of 1% WO_3/CMK-3 cathode reached 3.84 mg cm^{-2} h^{-1} in gas diffusion aeration, which was 3.3 times that in normal aeration. The Faradaic efficiency of the as-prepared cathode achieved 68% in gas diffusion aeration, which was 34.2% higher than that in normal aeration. Subsequently, the current of the as-prepared cathode was monitored in different aeration modes (Fig. 5(f)), which showed that the current was significantly higher in gas diffusion aeration, corresponding to its higher H_2O_2 production performance.

Since the refresh of the electrolyte can immediately replenish H^+ and transfer the generated H_2O_2, and then facilitating the oxygen reduction reaction to produce H_2O_2, the exploration of the effect of electrolyte flow rate on H_2O_2 production was significant. As displayed in Fig. S14 (a), the H_2O_2 production rate increased from 2.18 to 3.84 mg cm^{-2} h^{-1} as the electrolyte flow rate varied from 2 to 10 mL min^{-1}, and the Faradaic efficiency increased from 41% to 70%, which were consistent with the expected results. As oxygen mass transfer at the cathodic reaction interface is an important factor for achieving efficient H_2O_2 production [48], the influence of the O_2 flow rate on H_2O_2 production was investigated. The results showed that both the H_2O_2 production rate and the Faradaic efficiency increased as the O_2 flow rate increased from 20 to 100 mL min^{-1} (Fig. S14(b)), confirming the significant effect of mass transfer of oxygen on the H_2O_2 production. In addition, the effect of the initial solution pH on the H_2O_2 production was tested. As depicted in Fig. S14(c), the H_2O_2 production rate of 1% WO_3/CMK-3 cathode increased from 2.46 to 3.84 mg cm^{-2} h^{-1} as the solution pH decreased from 8 to 2. High H_2O_2 yields were obtained on the cathode with low pH, which can be explained by the participation of H^+ in H_2O_2 generation and H_2O_2 decomposition at alkaline pH ($2\,H_2O_2 \rightarrow 2\,H_2O + O_2$). In addition, the W dissolution in the WO_3/CMK-3 cathode during operation (pH=8) may be another reason, as analyzed by Inductively Coupled Plasma Optical-Emission Spectroscopy (ICP-OES) in Fig. S15. Notably, the Faradaic efficiency of WO_3/CMK-3 cathode does not vary with pH conditions (68–69%), and the more negative current density of the electrode at a lower pH could explain this phenomenon (CV curves in Fig. S14(d)). These results indicated that the WO_3/CMK-3 cathode exhibited high H_2O_2 production activity at different pH values, which will be a promising cathode used for H_2O_2 production and synergistic wastewater treatment on the anode.

3.3. Total nitrogen removal of urine

According to Eqs. (2) and 3, the urea decomposition is an exothermic process, while the reduction of oxygen to H_2O_2 is an endothermic process, which indicates that the chemical energy released from urea decomposition may be utilized by the reaction of oxygen reduction to produce H_2O_2 (Eq. (4)). Based on this, a novel method based on a self-biased WO_3/TiO_2-Si PVC photoanode and a WO_3/CMK-3 cathode was proposed, which aimed at producing the high value-added chemical H_2O_2 from efficient total nitrogen removal of urine. The mechanism of urine treatment and synergistic H_2O_2 production was shown in Fig. S3. The Si PVC was adhered to the back of the WO_3/TiO_2 and sealed by silicone rubber to form a self-biased composite photoanode. With a type-II interface band structure, the front WO_3/TiO_2 photoanode can reduce the possibility of surface trap recombination and improve the separation of electron-hole pairs. Moreover, the WO_3/TiO_2 absorbs mainly the

short-wavelength part of sunlight (< 460 nm) and the filtered long-wavelength light (> 460 nm) can be captured by rear Si PVC, which could simultaneously expand the absorption portion of the solar spectrum and strengthen the separation and migration of charges in the PEC system [32]. Due to the bias of Si PVC, the oxidation capacity of the WO_3/TiO_2 photoanode can be greatly enhanced. The experiments of synthetic urine degradation on WO_3/TiO_2-Si PVC photoanode and synergistic H_2O_2 generation on 1% WO_3/CMK-3 cathode were performed. As shown in Figs. 6(a), 90.8% of urea can be removed within 60 min at pH 3. However, the TN removal rate was 78.7–88.8% when pH was 5–9. The increase of solution pH leads to decreased urea removal efficiency. At pH 3, the kinetic constant (k) for urea degradation is 0.0390 min^{-1}, which decreases to 0.0266 min^{-1} at pH 9 (Fig. 6(b)). The pH-dependent degradation rate can be ascribed to that the lower pH of anolyte can replenish H^+ for catholyte and then facilitate cathodic H_2O_2 production, which in turn promote the exothermic reaction of urea decomposition. Moreover, WO_3/TiO_2 seems to perform better under acidic conditions, which is responsible for the poor degradation of urea at higher pH [49].

Since the oxidation of urea at the anode is a kinetically slow process and prone to excessive oxidation to nitrate nitrogen [5,50], and the free chlorine is considered to be the main factor in urea oxidation according to the Volmer-Heyrovsky mechanism [51], it is crucial to investigate the effect of chlorine concentration on urea degradation efficiency. Fig. 6(c) illustrated the urea removal at different initial chloride concentrations. As shown in the results, the addition of chloride remarkably boosted the removal rate of urea. The oxidation process of urea without the addition of chloride was very slow (15.3%). As the chloride concentration increased from 0.03 to 0.07 M, the urea degradation efficiency was significantly improved from 60.8% to 91.0%. The degradation of urea followed the pseudo-first-order kinetic principle (Fig. 6(d)), and the kinetic constant was 0.0397 min^{-1} at a Cl^- concentration of 0.07 M, which was 2.5 times than that at 0.03 M Cl^- (0.0160 min^{-1}) and 15.4 times than that at 0 M Cl^- (0.00258 min^{-1}). The TN removal rates of synthetic urine at different Cl^- concentrations were also monitored, and the results showed that the TN removal rate increased from 11.9% to 78.1% when Cl^- was increased from 0 to 0.07 M (Fig. 6(f)), which corresponded to the urea degradation efficiency. It is worth noting that the degradation and mineralization of urea did not increase significantly when the chloride concentration increased from 0.05 M to 0.07 M, which could be explained by the fact that higher Cl^- concentration may

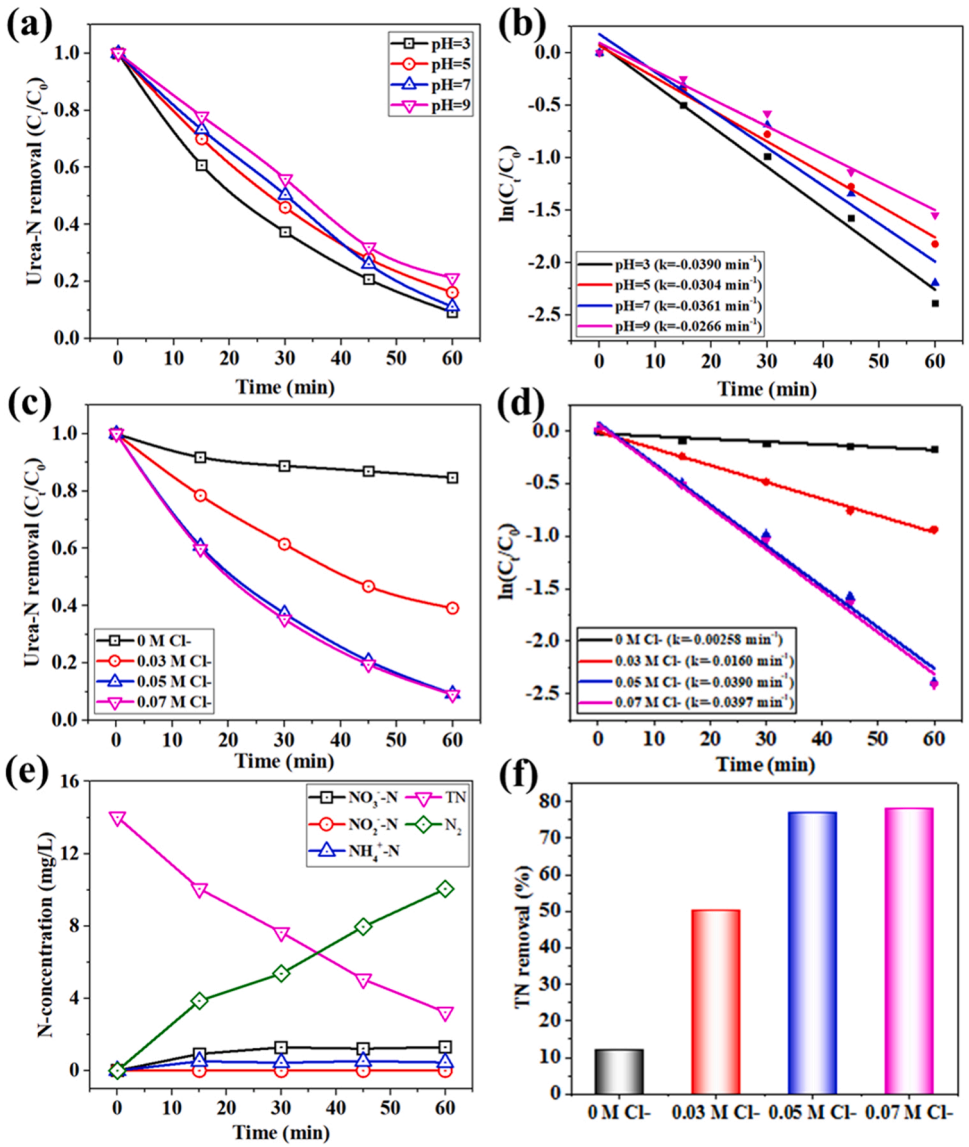

Fig. 6. Effect of (a) anolyte pH (0.05 M Cl^-) and (c) initial chloride concentration (pH=3) on the removal rate of urea in synthetic urine. (b) and (d) Corresponding plots of ln (C_t/C_0) versus time. (e) Different N-concentrations versus time during the degradation of synthetic urine, conditions: Anolyte: 30 mg L^{-1} urea, 0.1 M Na_2SO_4, 0.05 M NaCl, pH= 3; Catholyte: pH= 2, 0.1 M Na_2SO_4. (f) Effects of initial chloride concentration on TN removal.

lead to the high generation of NO_3^- [52].

To determine the variation of N species in urea degradation products, we monitored the concentrations of NO_3-N, NO_2-N, NH_3-N, TN, and N_2, and the results were shown in Fig. 6(e). After 60 min of degradation, the concentrations of NO_3-N and NH_3-N accumulated to 1.3 and 0.45 mg L^{-1}, respectively. The NO_2-N has never been detected (below the instrument detection limit) because it can be easily oxidized in a strong oxidation environment. 76.9% of TN was removed at 60 min, indicating that the majority of the nitrogen was mineralized into the harmless N_2 during the degradation of synthetic urine (71.6%), which demonstrated the excellent urine treatment capacity of the constructed PEC system.

To explore the H_2O_2 production capacity of the cathode during the treatment of synthetic urine in this system, the H_2O_2 yield and the Faradaic efficiency of the cathode with or without the removal of urea in the anode chamber were compared. As shown in Fig. 7(a), the cathodic H_2O_2 production rate reached 5.13 mg cm^{-2} h^{-1} in the anodic solution containing 0.1 M Na_2SO_4, 0.05 M NaCl and 30 mg L^{-1} urea, nearly 1.34 times higher than the initial production rate (3.84 mg cm^{-2} h^{-1}) in 0.1 M Na_2SO_4.

This indicated that the removal of urea had a remarkable synergistic effect on H_2O_2 production, in which the potential energy released from urea degradation was recovered to form H_2O_2, and the generated electrons were efficiently captured by the cathode to participate in the oxygen reduction reaction. Moreover, several studies have also reported the feasibility of pollutant degradation to provide electrons for cathodic reduction reactions [53]. The LSV plots in Fig. 7(b) showed that the 1% WO_3/CMK-3 cathode has a higher current in the presence of urea in anolyte, which corresponded to a higher urea removal rate and H_2O_2 production rate.

3.4. Mechanisms of H_2O_2 production from urine treatment

Based on the above analysis, a possible mechanism for treating urine wastewater in the self-biased PEC system was proposed and schematically depicted in Fig. S3. To explore the existence of radicals, we investigated the radical species by electron spin resonance spectroscopy (ESR) using 5,5-dimethyl-1-pyrroline N-oxide (DMPO) as a trapping agent. The clear quartet peaks of •OH with 1:2:2:1 intensity could be observed in the system without chlorine (Fig. 7(c)). When inducing Cl^- in the PEC system, seven new peaks emerged, which corresponded to the DMPO-Cl• [22]. We then used different scavengers to investigate the role of Cl• in urea degradation (TBA for •OH and Cl•, NB for •OH) [54]. As shown in Fig. 7(d), urea degradation was suppressed obviously after adding TBA, which demonstrated that Cl• and •OH were both involved. While urea degradation was slightly inhibited by adding NB, suggesting that the role of •OH was limited. Therefore, Cl•-mediated radical oxidation played a major role in urea degradation (54.6%).

The self-bias voltage generated between the Si PVC and the WO_3/TiO_2 drove the electron migration from the WO_3/TiO_2 photoanode to the 1% WO_3/CMK-3 cathode, effectively promoting the formation of •OH/Cl• on the photoanode and the production of H_2O_2 on the cathode. Under light irradiation, WO_3/TiO_2 photoanode generated photoexcited electron-hole pairs (h^+-e^-), and then h^+ was captured by Cl^- to form Cl•. Cl• dominated the oxidation of urea and rapidly oxidized urea into an amine group (-NH_2) and then converted NH_2• into N_2 together with HClO. Meanwhile, a cycle between Cl^- and Cl• was achieved (Eqs. (13)-(19)). In addition, organic matter in urine was mineralized by •OH into CO_2 and H_2O (Eq. (20)) and trace amounts of the amino group were oxidized to NO_3^- (Eqs. (21) and (22)).

$$WO_3/TiO_2 + h\nu \rightarrow h^+ + e^- \quad (7)$$

$$H_2O + h^+ \rightarrow \bullet OH + H^+ \quad (8)$$

$$Cl^- + h^+ \rightarrow Cl\bullet \; k = 1{\cdot}8 \times 10^{10}\ M^{-1}\ s^{-1} \quad (9)$$

$$Cl^- + \bullet OH \rightarrow Cl\bullet + OH^- \; k = 4{\cdot}3 \times 10^{9}\ M^{-1}\ s^{-1} \quad (10)$$

$$Cl\bullet + Cl^- \rightarrow Cl_2\bullet^- k = 8{\cdot}0 \times 10^{9}\ M^{-1}\ s^{-1} \quad (11)$$

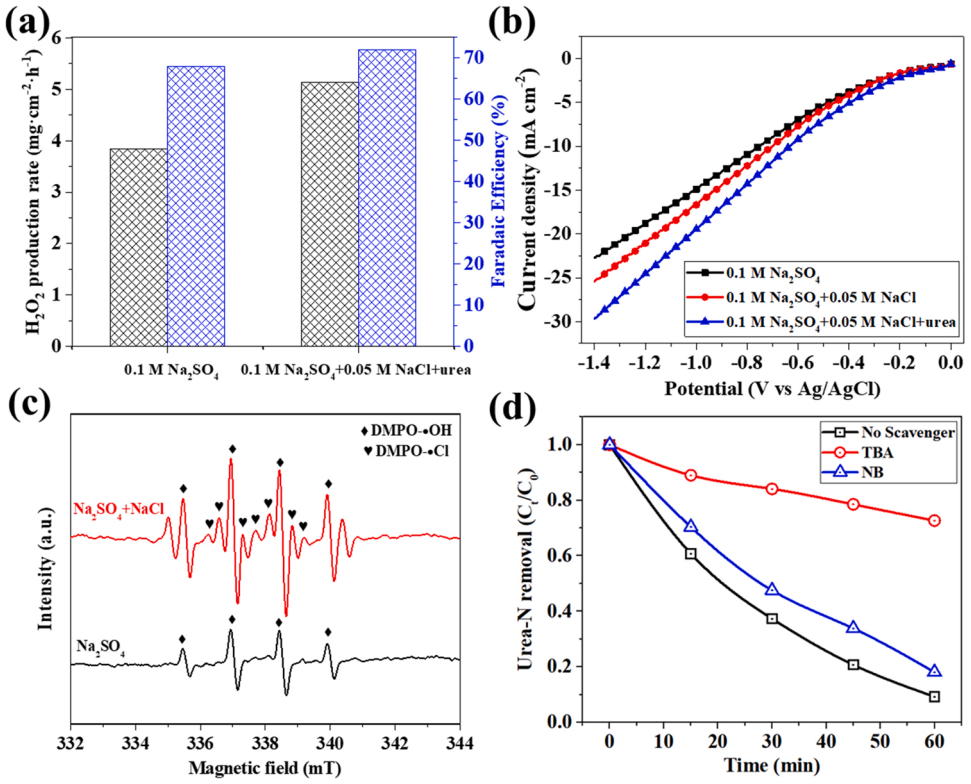

Fig. 7. (a) H_2O_2 yield and Faradaic efficiency, and (b) current density of WO_3/CMK-3 electrode in different systems. (c) ESR spectra during the urea removal process. (d) Related experiments of free radical quenching. Conditions: Anolyte: 30 mg L^{-1} urea, 0.1 M Na_2SO_4, 0.05 M NaCl, pH= 3; Catholyte: pH= 2, 0.1 M Na_2SO_4.

$$Cl_2\bullet^- + H_2O \rightarrow 2\,H^+ + ClO^- + Cl^-\ k = 2{\cdot}5 \times 10^8\ M^{-1}\ s^{-1} \quad (12)$$

$$NH_2CONH_2 + 2Cl\bullet + H_2O \rightarrow 2NH_2\bullet + 2Cl^- + 2\,H^+ + CO_2 \quad (13)$$

$$NH_2\bullet + HClO \rightarrow NH_2Cl + \bullet OH \quad (14)$$

$$NH_2Cl + Cl\bullet \rightarrow \bullet NHCl + Cl^- + H^+ \quad (15)$$

$$\bullet NHCl + HClO \rightarrow NHCl_2 + \bullet OH \quad (16)$$

$$NHCl_2 + NH_2Cl \rightarrow N_2 + 3\,H^+ + 3Cl^- \quad (17)$$

$$NHCl_2 + H_2O \rightarrow NOH + 2\,H^+ + 2Cl^- \quad (18)$$

$$NHCl_2 + NOH \rightarrow N_2 + HClO + H^+ + Cl^- \quad (19)$$

$$RH + \bullet OH \rightarrow R\bullet + O_2 \rightarrow \cdots CO_2 + H_2O \quad (20)$$

$$NH_2\bullet + \bullet OH \rightarrow NH_2OH \quad (21)$$

$$NH_2OH + \bullet OH \rightarrow NO_2^- \rightarrow NO_3^- \quad (22)$$

Photoelectrochemical synthesis of H_2O_2 from oxygen reduction reaction (ORR) proceeds mainly via a $2e^-$ transfer pathway (Eq. (23)) [55]. However, oxygen molecules can also be reduced to H_2O via the direct $4e^-$ pathway (Eq. (24)). To achieve efficient H_2O_2 production, seeking a highly selective cathode catalyst is necessary [56–58]. In this case, the WO_3-modified CMK-3 cathode (WO_3/CMK-3) was prepared in this study due to its high specific surface area and hydrophilic/hydrophobic interface, which gives it a large number of catalytic active sites and efficient O_2 transfer channels for efficient H_2O_2 production. According to Eq. (4), H_2O_2 production from urine treatment is a process with a strong thermodynamic spontaneous trend, which indicates that a feasible reversal of the thermodynamic trend of O_2 reduction to H_2O_2 from non-spontaneous to strong spontaneous can be achieved by combining it with a urine treatment reaction that releases large amounts of chemical energy in a photoelectrocatalytic system. Besides, the electrons generated from urine oxidation were also transferred to the WO_3/CMK-3 cathode via an external circuit, which can further enhance the H_2O_2 production.

$$O_2 + 2\,H^+ + 2\,e^- \rightarrow H_2O_2\ 0{\cdot}695\ V\ vs{\cdot}RHE \quad (23)$$

$$O_2 + 4\,H^+ + 4\,e^- \rightarrow 2\,H_2O\ 1{\cdot}230\ V\ vs{\cdot}RHE \quad (24)$$

3.5. Actual urine treatment and cycling performance tests

To demonstrate the practicality and durability of the PEC system, experiments of actual urine treatment were performed. The actual urine samples were collected from a public latrine, which were filtered and diluted for immediate disposal. The physicochemical properties of actual urine samples were presented in Table S2. As shown in Figs. 8(a), 91.4% of TN was removed from the actual urine after 120 min of reaction. Moreover, the TN removal rate of urine samples was still as high as 82.8% after ten accumulated tests, which indicates that the WO_3/TiO_2 photoanode has good treatment capability. The durability of the 1% WO_3/CMK-3 cathode was also evaluated by repeated H_2O_2 production experiments. In Fig. 8(b), the H_2O_2 yield and Faradaic efficiency of 1% WO_3/CMK-3 cathode nearly remained the same as the fresh sample after ten consecutive cycles (5 mg cm^{-2} h^{-1} and 71%), which demonstrates that 1% WO_3/CMK-3 cathode has good stability. In addition, the morphology of the used WO_3/TiO_2 photoanode and 1% WO_3/CMK-3 cathode was found to be similar to that of fresh ones (Fig. S16). All these results illustrated that the fabricated PEC system possessed good durability, which had a potential for long-term application in the actual urine treatment.

4. Conclusions

The major sources of nitrogen pollution in wastewater treatment plants propose a great challenge for wastewater treatment. Efficient denitrification and resource utilization of urine through source separation is an effective way to mitigate urine pollution. Based on this, a novel bi-functional PEC system was constructed to realize simultaneous nitrogen removal and H_2O_2 production in urine wastewater treatment. In this study, a WO_3/TiO_2-Si PVC composite photoanode was prepared to generate •OH/Cl• for the highly selective conversion of urine to N_2 and CO_2. The chemical energy released from the denitrogenation of urine was subsequently recovered by the thermodynamically unfavorable reduction of O_2 to H_2O_2 on the WO_3/CMK-3 cathode. Results indicated the degradation efficiency of synthetic urine within 60 min was 91.0%, and 91.4% of TN was removed from the actual urine after 120 min of reaction. The system also showed a superior performance for H_2O_2 production with a yield of 5.13 mg cm^{-2} h^{-1} in 60 min. Combined with the analysis of ESR and free radical capture experiment, it was concluded that Cl• played an important role in urea oxidation. The results demonstrated that the proposed PEC system offers a foundation for the simultaneous efficient purification and resource utilization of urine.

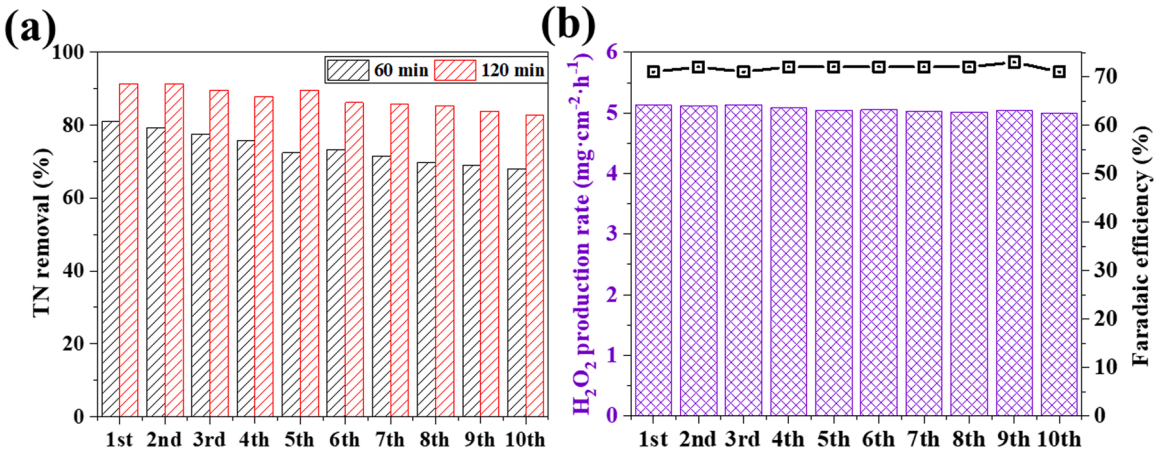

Fig. 8. (a) The stability test of the WO_3/TiO_2 photoanode used for TN removal of actual urine wastewater. Conditions : Anolyte: pH = 3, 0.1 M Na_2SO_4 + 0.05 M NaCl; Catholyte: pH = 2, 0.1 M Na_2SO_4. (b) The stability test of the WO_3/CMK-3 cathode was used for H_2O_2 generation. Conditions : Anolyte: pH = 3, 0.1 M Na_2SO_4 + 0.05 M NaCl, 30 mg L^{-1} urea; Catholyte: pH = 2, 0.1 M Na_2SO_4.

CRediT authorship contribution statement

Lei Li: Conceptualization, Data curation, Writing – original draft, Writing – review & editing. **Jinhua Li:** Visualization, Investigation, Supervision. **Fei Fang:** Investigation, Data curation. **Yan Zhang:** Investigation, Data curation, Methodology. **Tingsheng Zhou:** Methodology. **Changhui Zhou:** Methodology. **Jing Bai:** Visualization, Supervision. **Baoxue Zhou:** Conceptualization, Supervision, Project administration, Writing – review & editing.

Declaration of Competing Interest

The authors declare that they have no known competing financial interests or personal relationships that could have appeared to influence the work reported in this paper.

Data Availability

Data will be made available on request.

Acknowledgments

The authors would like to acknowledge the National Natural Science Foundation of China (No. 22178220, 52200103, 22176125), the Fundamental Research Funds for the Central Universities, the Center for Advanced Electronic Materials and Devices (AEMD), and the instrumental Analysis Center (SESE) of Shanghai Jiao Tong University (SJTU) for support.

Appendix A. Supporting information

Supplementary data associated with this article can be found in the online version at doi:10.1016/j.apcatb.2023.122776.

References

[1] E. Sinha, A.M. Michalak, V. Balaji, Eutrophication will increase during the 21st century as a result of precipitation changes, Sci 357 (2017) 405–408, https://doi.org/10.1126/science.aan2409.
[2] V. Amstutz, A. Katsaounis, A. Kapalka, C. Comninellis, K.M. Udert, Effects of carbonate on the electrolytic removal of ammonia and urea from urine with thermally prepared IrO_2 electrodes, J. Appl. Electrochem. 42 (2012) 787–795, https://doi.org/10.1007/s10800-012-0444-y.
[3] K.A. Landry, T.H. Boyer, Life cycle assessment and costing of urine source separation: focus on nonsteroidal anti-inflammatory drug removal, Water Res. 105 (2016) 487–495, https://doi.org/10.1016/j.watres.2016.09.024.
[4] J. Zhang, Q. She, V.W.C. Chang, C.Y. Tang, R.D. Webster, Mining nutrients (N, K, P) from urban source-separated urine by forward osmosis dewatering, Environ. Sci. Technol. 48 (2014) 3386–3394, https://doi.org/10.1021/es405266d.
[5] X.-J. Xu, H.-J. Li, W. Wang, R.-C. Zhang, X. Zhou, D.-F. Xing, N.-Q. Ren, D.-J. Lee, Y.-X. Yuan, L.-H. Liu, C. Chen, The performance of simultaneous denitrification and biogas desulfurization system for the treatment of domestic sewage, Chem. Eng. J. 399 (2020), 125855, https://doi.org/10.1016/j.cej.2020.125855.
[6] L. Gao, F. Han, X. Zhang, B. Liu, D. Fan, X. Sun, Y. Zhang, L. Yan, D. Wei, Simultaneous nitrate and dissolved organic matter removal from wastewater treatment plant effluent in a solid-phase denitrification biofilm reactor, Bioresour. Technol. 314 (2020), 123714, https://doi.org/10.1016/j.biortech.2020.123714.
[7] C. Courtney, D.G. Randall, Concentrating stabilized urine with reverse osmosis: How does stabilization method and pre-treatment affect nutrient recovery, flux, and scaling, Water Res. 209 (2022), 117970, https://doi.org/10.1016/j.watres.2021.117970.
[8] C. Xue, L.D. Wilson, Kinetic study on urea uptake with chitosan based sorbent materials, Carbohydr. Polym. 135 (2016) 180–186, https://doi.org/10.1016/j.carbpol.2015.08.090.
[9] Y. Peng, G. Zhu, Biological nitrogen removal with nitrification and denitrification via nitrite pathway, Appl. Microbiol. Biotechnol. 73 (2006) 15–26, https://doi.org/10.1007/s00253-006-0534-z.
[10] W. Simka, J. Piotrowski, A. Robak, G. Nawrat, Electrochemical treatment of aqueous solutions containing urea, J. Appl. Electrochem. 39 (2009) 1137–1143, https://doi.org/10.1007/s10800-008-9771-4.
[11] E. Urbańczyk, M. Sowa, W. Simka, Urea removal from aqueous solutions—a review, J. Appl. Electrochem. 46 (2016) 1011–1029, https://doi.org/10.1007/s10800-016-0993-6.
[12] G. Ye, P. Luo, Y. Zhao, G. Qiu, Y. Hu, S. Preis, C. Wei, Three-dimensional Co/Ni bimetallic organic frameworks for high-efficient catalytic ozonation of atrazine: mechanism, effect parameters, and degradation pathways analysis, Chemosphere 253 (2020), 126767, https://doi.org/10.1016/j.chemosphere.2020.126767.
[13] M. Zeng, J. Wu, Z. Li, H. Wu, J. Wang, H. Wang, L. He, X. Yang, Interlayer effect in NiCo layered double hydroxide for promoted electrocatalytic urea oxidation, ACS Sustain. Chem. Eng. 7 (2019) 4777–4783, https://doi.org/10.1021/acssuschemeng.8b04953.
[14] C. Zhou, J. Bai, Y. Zhang, J. Li, Z. Li, P. Jiang, F. Fang, M. Zhou, X. Mei, B. Zhou, Novel 3D Pd-Cu$(OH)_2$/CF cathode for rapid reduction of nitrate-N and simultaneous total nitrogen removal from wastewater, J. Hazard. Mater. 401 (2021), 123232, https://doi.org/10.1016/j.jhazmat.2020.123232.
[15] W. Zheng, S. You, Y. Yao, N. Ren, B. Ding, F. Li, Y. Liu, Sustainable generation of sulfate radicals and decontamination of micropollutants via sequential electrochemistry, Engineering (2023), https://doi.org/10.1016/j.eng.2022.12.005.
[16] J.A. Wilsenach, M.C.M.Van Loosdrecht, Effects of separate urine collection on advanced nutrient removal processes, Environ. Sci. Technol. 38 (2004) 1208–1215, https://doi.org/10.1021/es0301018.
[17] T.A. Larsen*, A.C. Alder, R.I.L. Eggen, M. Maurer, J. Lienert, Source separation: will we see a paradigm shift in wastewater handling? Environ. Sci. Technol. 43 (2009) 6121–6125, https://doi.org/10.1021/es803001r.
[18] B.K. Boggs, R.L. King, G.G. Botte, Urea electrolysis: direct hydrogen production from urine, Chem. Commun. (2009) 4859–4861, https://doi.org/10.1039/B905974A.
[19] H. Zhao, Y. Zhang, C. Xie, J. Wang, T. Zhou, C. Zhou, J. Li, J. Bai, X. Zhu, B. Zhou, Facile, controllable, and ultrathin NiFe-LDH in situ grown on a Ni FOam by Ultrasonic Self-etching for Highly Efficient Urine Conversion, Environ. Sci. Technol. 57 (2023) 2939–2948, https://doi.org/10.1021/acs.est.2c07282.
[20] Y. Zhang, X. Huang, J. Li, J. Bai, C. Zhou, L. Li, J. Wang, M. Long, X. Zhu, B. Zhou, Rapid conversion of Co^{2+} to Co^{3+} by introducing oxygen vacancies in Co_3O_4 nanowire anodes for nitrogen removal with highly efficient H_2 recovery in urine treatment, Environ. Sci. Technol. 56 (2022) 9693–9701, https://doi.org/10.1021/acs.est.2c00729.
[21] C. Zhou, J. Li, J. Wang, C. Xie, Y. Zhang, L. Li, T. Zhou, J. Bai, H. Zhu, B. Zhou, Efficient H_2 production and TN removal for urine disposal using a novel photoelectrocatalytic system of $Co_3O_4/BiVO_4$ - MoNiCuOx/Cu, Appl. Catal. B-Environ. 324 (2023), 122229, https://doi.org/10.1016/j.apcatb.2022.122229.
[22] Z. Shen, J. Li, Y. Zhang, J. Bai, X. Tan, X. Li, L. Qiao, Q. Xu, B. Zhou, Highly efficient total nitrogen and simultaneous total organic carbon removal for urine based on the photoelectrochemical cycle reaction of chlorine and hydroxyl radicals, Electrochim. Acta 297 (2019) 1–9, https://doi.org/10.1016/j.electacta.2018.11.087.
[23] X. Wang, M. Sun, Y. Zhao, C. Wang, W. Ma, M.S. Wong, M. Elimelech, In situ electrochemical generation of reactive chlorine species for efficient ultrafiltration membrane self-cleaning, Environ. Sci. Technol. 54 (2020) 6997–7007, https://doi.org/10.1021/acs.est.0c01590.
[24] W. Duan, G. Li, Z. Lei, T. Zhu, Y. Xue, C. Wei, C. Feng, Highly active and durable carbon electrocatalyst for nitrate reduction reaction, Water Res. 161 (2019) 126–135, https://doi.org/10.1016/j.watres.2019.05.104.
[25] Y. Zhang, Y. Ji, J. Li, J. Bai, S. Chen, L. Li, J. Wang, T. Zhou, P. Jiang, X. Guan, B. Zhou, Efficient ammonia removal and toxic chlorate control by using $BiVO_4$/WO_3 heterojunction photoanode in a self-driven PEC-chlorine system, J. Hazard. Mater. 402 (2021), 123725, https://doi.org/10.1016/j.jhazmat.2020.123725.
[26] Z. Shen, J. Bai, Y. Zhang, J. Li, T. Zhou, J. Wang, Q. Xu, B. Zhou, Efficient purification and chemical energy recovery from urine by using a denitrifying fuel cell, Water Res. 152 (2019) 117–125, https://doi.org/10.1016/j.watres.2018.12.066.
[27] Z. Shen, Y. Zhang, C. Zhou, J. Bai, S. Chen, J. Li, J. Wang, X. Guan, M. Rahim, B. Zhou, Exhaustive denitrification via chlorine oxide radical reactions for urea based on a novel photoelectrochemical cell, Water Res. 170 (2020), 115357, https://doi.org/10.1016/j.watres.2019.115357.
[28] J.K. Edwards, B. Solsona, E.N. N, A.F. Carley, A.A. Herzing, C.J. Kiely, G. J. Hutchings, Switching off hydrogen peroxide hydrogenation in the direct synthesis process, Sci 323 (2009) 1037–1041, https://doi.org/10.1126/science.1168980.
[29] J. Zhang, G. Zhang, Q. Ji, H. Lan, J. Qu, H. Liu, Carbon nanodot-modified FeOCl for photo-assisted Fenton reaction featuring synergistic in-situ H_2O_2 production and activation, Appl. Catal. B-Environ. 266 (2020), 118665, https://doi.org/10.1016/j.apcatb.2020.118665.
[30] J.M. Campos-Martin, G. Blanco-Brieva, J.L.G. Fierro, Hydrogen peroxide synthesis: an outlook beyond the anthraquinone process, Angew. Chem. Int. Ed. 45 (2006) 6962–6984, https://doi.org/10.1002/anie.200503779.
[31] M.H.M.T. Assumpção, R.F.B. De Souza, R.M. Reis, R.S. Rocha, J.R. Steter, P. Hammer, I. Gaubeur, M.L. Calegaro, M.R.V. Lanza, M.C. Santos, Low tungsten content of nanostructured material supported on carbon for the degradation of phenol, Appl. Catal. B-Environ., 142- 143 (2013) 479–486, https://doi.org/10.1016/j.apcatb.2013.05.024.
[32] Q. Zeng, J. Bai, J. Li, B. Zhou, Y. Sun, A low-cost photoelectrochemical tandem cell for highly-stable and efficient solar water splitting, Nano Energy 41 (2017) 225–232, https://doi.org/10.1016/j.nanoen.2017.09.032.
[33] S.S. Kalanur, Y.J. Hwang, S.Y. Chae, O.S. Joo, Facile growth of aligned WO_3 nanorods on FTO substrate for enhanced photoanodic water oxidation activity, J. Mater. Chem. A 1 (2013) 3479, https://doi.org/10.1039/c3ta01175e.
[34] L. Li, J. Bai, S. Chen, Y. Zhang, J. Li, T. Zhou, J. Wang, X. Guan, B. Zhou, Enhanced O_2− and HO via in situ generating H_2O_2 at activated graphite felt cathode for efficient photocatalytic fuel cell, Chem. Eng. J. 399 (2020), 125839, https://doi.org/10.1016/j.cej.2020.125839.

[35] X. Shi, Y. Zhang, S. Siahrostami, X. Zheng, Light-driven $BiVO_4$–C fuel cell with simultaneous production of H_2O_2, Adv. Energy Mater. 8 (2018) 1801158, https://doi.org/10.1002/aenm.201801158.
[36] Y. Sun, I. Sinev, W. Ju, A. Bergmann, S. Dresp, S. Kühl, C. Spöri, H. Schmies, H. Wang, D. Bernsmeier, B. Paul, R. Schmack, R. Kraehnert, B. Roldan Cuenya, P. Strasser, Efficient electrochemical hydrogen peroxide production from molecular oxygen on nitrogen-doped mesoporous carbon catalysts, ACS Catal. 8 (2018) 2844–2856, https://doi.org/10.1021/acscatal.7b03464.
[37] Z. Lu, G. Chen, S. Siahrostami, Z. Chen, K. Liu, J. Xie, L. Liao, T. Wu, D. Lin, Y. Liu, T.F. Jaramillo, J.K. Nørskov, Y. Cui, High-efficiency oxygen reduction to hydrogen peroxide catalysed by oxidized carbon materials, Nat. Catal. 1 (2018) 156–162, https://doi.org/10.1038/s41929-017-0017-x.
[38] Q. Zhang, M. Zhou, G. Ren, Y. Li, Y. Li, X. Du, Highly efficient electrosynthesis of hydrogen peroxide on a superhydrophobic three-phase interface by natural air diffusion, Nat. Commun. 11 (2020) 1731, https://doi.org/10.1038/s41467-020-15597-y.
[39] M. Mazzucato, C. Durante, Insights on oxygen reduction reaction to H_2O_2: the role of functional groups and textural properties on the activity and selectivity of doped carbon electrocatalysts, Curr. Opin. Electro 35 (2022), 101051, https://doi.org/10.1016/j.coelec.2022.101051.
[40] J. Wang, T. Zhou, Y. Zhang, S. Chen, J. Bai, J. Li, H. Zhu, B. Zhou, The design of high performance photoanode of CQDs/TiO_2/WO_3 based on DFT alignment of lattice parameter and energy band, and charge distribution, J. Colloid Interface Sci. 600 (2021) 828–837, https://doi.org/10.1016/j.jcis.2021.05.086.
[41] T. Zhou, S. Chen, L. Li, J. Wang, Y. Zhang, J. Li, J. Bai, L. Xia, Q. Xu, M. Rahim, B. Zhou, Carbon quantum dots modified anatase/rutile TiO_2 photoanode with dramatically enhanced photoelectrochemical performance, Appl. Catal. B Environ. 269 (2020), 118776, https://doi.org/10.1016/j.apcatb.2020.118776.
[42] T. Zhou, L. Li, J. Li, J. Wang, J. Bai, L. Xia, Q. Xu, B. Zhou, Electrochemically reduced TiO_2 photoanode coupled with oxygen vacancy-rich carbon quantum dots for synergistically improving photoelectrochemical performance, Chem. Eng. J. 425 (2021), 131770, https://doi.org/10.1016/j.cej.2021.131770.
[43] C. Zhou, J. Li, Y. Zhang, J. Bai, L. Li, X. Mei, X. Guan, B. Zhou, Novel denitrification fuel cell for energy recovery of nitrate-N and TN removal based on NH_4^+ generation on a CNW@CF cathode, Environ. Sci. Technol. 56 (2022) 2562–2571, https://doi.org/10.1021/acs.est.1c04363.
[44] E.C. Paz, L.R. Aveiro, V.S. Pinheiro, F.M. Souza, V.B. Lima, F.L. Silva, P. Hammer, M.R.V. Lanza, M.C. Santos, Evaluation of H_2O_2 electrogeneration and decolorization of orange II azo dye using tungsten oxide nanoparticle-modified carbon, Appl. Catal. B-Environ. 232 (2018) 436–445, https://doi.org/10.1016/j.apcatb.2018.03.082.
[45] L. Li, J. Bai, P. Jiang, Y. Zhang, T. Zhou, J. Wang, C. Zhou, J. Li, B. Zhou, Efficient H_2O_2 electrosynthesis and its electro-fenton application for refractory organics degradation, Engineering (2023), https://doi.org/10.1016/j.eng.2023.02.005.
[46] S.Ng Eroi, A.S. Ello, D. Diabaté, D.B. Ossonon, Heterogeneous WO_3/H_2O_2 system for degradation of Indigo Carmin dye from aqueous solution, South Afr. J. Chem. Eng. 37 (2021) 53–60, https://doi.org/10.1016/j.sajce.2021.03.009.
[47] M.H.M.T. Assumpção, A. Moraes, R.F.B. De Souza, I. Gaubeur, R.T.S. Oliveira, V. S. Antonin, G.R.P. Malpass, R.S. Rocha, M.L. Calegaro, M.R.V. Lanza, M.C. Santos, Low content cerium oxide nanoparticles on carbon for hydrogen peroxide electrosynthesis, Appl. Catal. A-Gen., 411- 412 (2012) 1–6, https://doi.org/10.1016/j.apcata.2011.09.030.
[48] F. Yin, Y. Liu, C. Wang, H. Liu, Assessing the electron transfer and oxygen mass transfer of the oxygen reduction reaction using a new electrode kinetic equation, Phys. Chem. Chem. Phys. 20 (2018) 16159–16166, https://doi.org/10.1039/C8CP01305E.
[49] P. Lianos, Review of recent trends in photoelectrocatalytic conversion of solar energy to electricity and hydrogen, Appl. Catal. B-Environ. 210 (2017) 235–254, https://doi.org/10.1016/j.apcatb.2017.03.067.
[50] Z. He, Y. Tong, S. Ni, X. Ye, C.P. Makwarimba, X. Huang, S. Zhang, S. Song, Electrochemically reductive dechlorination of 3,6-dichloropicolinic acid on a palladium/nitrogen-doped carbon/nickel foam electrode, Electrochim. Acta 292 (2018) 685–696, https://doi.org/10.1016/j.electacta.2018.09.188.
[51] Y. Yang, J. Shin, J.T. Jasper, M.R. Hoffmann, Multilayer heterojunction anodes for saline wastewater treatment: design strategies and reactive species generation mechanisms, Environ. Sci. Technol. 50 (2016) 8780–8787, https://doi.org/10.1021/acs.est.6b00688.
[52] M. Yang, D. Lu, J. Yang, Y. Zhao, Q. Zhao, Y. Sun, H. Liu, J. Ma, Carbon and nitrogen metabolic pathways and interaction of cold-resistant heterotrophic nitrifying bacteria under aerobic and anaerobic conditions, Chemosphere 234 (2019) 162–170, https://doi.org/10.1016/j.chemosphere.2019.06.052.
[53] C. Guo, P. He, R. Cui, Q. Shen, N. Yang, G. Zhao, Electrochemical CO_2 reduction using electrons generated from photoelectrocatalytic phenol oxidation, Adv. Energy Mater. 9 (2019) 1900364, https://doi.org/10.1002/aenm.201900364.
[54] Y. Zhang, J. Li, J. Bai, X. Li, Z. Shen, L. Xia, S. Chen, Q. Xu, B. Zhou, Total organic carbon and total nitrogen removal and simultaneous electricity generation for nitrogen-containing wastewater based on the catalytic reactions of hydroxyl and chlorine radicals, Appl. Catal. B-Environ. 238 (2018) 168–176, https://doi.org/10.1016/j.apcatb.2018.07.036.
[55] Y. Xia, X. Zhao, C. Xia, Z.-Y. Wu, P. Zhu, J.Y. Kim, X. Bai, G. Gao, Y. Hu, J. Zhong, Y. Liu, H. Wang, Highly active and selective oxygen reduction to H_2O_2 on boron-doped carbon for high production rates, Nat. Commun. 12 (2021) 4225, https://doi.org/10.1038/s41467-021-24329-9.
[56] Y. Sun, L. Han, P. Strasser, A comparative perspective of electrochemical and photochemical approaches for catalytic H_2O_2 production, Chem. Soc. Rev. 49 (2020) 6605–6631, https://doi.org/10.1039/D0CS00458H.
[57] H. Tang, Y. Zeng, D. Liu, D. Qu, J. Luo, K. Binnemans, D.E. De Vos, J. Fransaer, D. Qu, S.-G. Sun, Dual-doped mesoporous carbon synthesized by a novel nanocasting method with superior catalytic activity for oxygen reduction, Nano Energy 26 (2016) 131–138, https://doi.org/10.1016/j.nanoen.2016.05.015.
[58] Y. Jiang, P. Ni, C. Chen, Y. Lu, P. Yang, B. Kong, A. Fisher, X. Wang, Selective electrochemical H_2O_2 production through two-electron oxygen electrochemistry, Adv. Energy Mater. 8 (2018) 1801909, https://doi.org/10.1002/aenm.201801909.